INTERACTION OF GROWING CRACKS IN HYDRAULIC FRACTURING

by

LI WEI LO

Presented to the Faculty of the Graduate School of

The University of Texas at Arlington in Partial Fulfillment

of the Requirements

for the Degree of

MASTER OF SCIENCE IN MECHANICAL ENGINEERING

THE UNIVERSITY OF TEXAS AT ARLINGTON

May 2014

Acknowledgements

I would like to thank my advisor, Professor Bo Yang, for all of his help in completing this thesis. My interest in fracture network was first piqued last winter when I stopped by Professor Yang's office. I was lucky enough to have the opportunity to learn from him throughout my graduate study. Thank you Professor Yang for always being available and open minded, and for making the thesis-writing process such an enjoyable experience. I could not have asked for better guidance. I would also like to thank Professor Chan, who introduced me to fundamental knowledge for solid mechanics and guided me in the first year of my graduate degree.

I am grateful to Dr. Wang and Dr. Chan for serving my thesis committee and evaluating my work.

Most importantly, I would like to thank my parents, Ying-Ying Lo and Wen-shin Chang, for their fully support and blessing. I thank my wife and her family, Iris Wang, and her family, for their love and understanding during my graduate study. I also thank to my brother, sister, and brother-in-law, Li-Hsing, Li-Ying, Jack Hu, being really helpful and supportive. I would like to thank my roommates Walter, being always positive to my attitude. I like to thank all of my friends, who always cheered me up when I was down.

April 21, 2014

Abstract

INTERACTION OF GROWING CRACKS IN HYDRAULIC FRACTURING

Li Wei Lo, MS

The University of Texas at Arlington, 2014

Supervising Professor: Bo Yang

Recently, hydraulic fracturing has been utilized to extract natural gas and oil from low-permeability shale rocks. This technique has been studied in hundreds of papers. A deep understanding of the fracture network formation in hydraulic fracturing is essential to advancing the technology, e.g., to enhance the quality of fracking, and to keep aquifers from being contaminated. In the present study, the Linear Elastic Fracture Mechanics (LEFM) is applied to approach the crack extension behaviors in brittle rocks under hydraulic loading. The boundary element method is used to carry out the simulation where numerical treatment is only needed upon the cracks and the boundaries. When cracks extend, only new elements are added, but no re-meshing is necessary. With an appropriate crack extension criterion, the problems of crack initiation, crack interaction, and crack arrest are studied. This effort provides the oil and gas industry with more knowledge and understanding of crack growth in fracking.

Table of Contents

List of Illustrations

List of Tables

Chapter 1

Introduction

Hydraulic fracturing has been a hot topic in recent years. The unconventional oil and gas revolution has revitalized the U.S economy regarding geoscience, oil gas, and engineering fields. Economically, some mid-west regions in the United States such as Montana and Texas have experienced an economy boom, clustering around the areas storing a large amount of shale gas formation, and the shale gas rush made the unemployment rate dropped to less than 1 percent in those two states. However, there are some downsides for shale gas extraction. Environmentally, the extraction of shale gas out of ground may pollute the water supply, an example happening in Pennsylvania. Although hydraulic fracturing is an old and well-known technique, the sophisticated crack network in hydraulic fracturing in shale gas has not been understood yet. The main point of this study is to make the hydraulic fracturing more controllable, which can benefit not only the oil company to improve the efficiency of this technique in shale gas, but also the oil company to prevent contaminating the environment. As a result, the objective in my thesis study is to understand crack initiation and the crack propagation, and the complicated crack network.

1.1 Drilling Completion Process

The initial step is about the same as conventional drilling. The hole is drilled vertically straight down by pumping water based fluid, which cools the drill bed, carries the rock back to the surface, and stabilizes the surface of the wellbore. Once the well extends over the deepest fresh water aquifer, the drill pipe is removed, and it is replaced with steel pipe called casing. This casing is cemented in place, and provides a multi-layer barrier to protect fresh water aquifer. The process for steel pipe is first pump cement down to casing until reaching the bottom. The cement flows between the casing and bore hole well, which creates an impermeable additive barrier, and can prevent the casing from contacting any water source. Second step is to continuously drill vertically until the kick-off point. The kick-off point is where the drilling becomes horizontal. The key point for horizontal drilling is to make several wells in one drill, and then minimize the impact for the environment. When the targeted area is reached, the drill pipe is removed. The steel casing is cemented to the additional full length of wellbore. Third step is to load a perforated gun in order to make crack initiation. Perforated gun is fired, and the perforated hole is connected to cement and the rock reservoir. The perforated gun is removed. The next step is hydraulic fracturing, which injects typically millions gallons of water mixed with sand and chemicals, and some mixture as lubricant under high pressure into a wellbore to increase pressure down hole at the targeted zone and also kill bacteria. Some papers have mentioned to optimize the fluid viscosity that can contribute highly extracted rate of shale gas. The sand is to keep the fractured hole open within 1centimeter when the pumping is relieved. This allows the gas flows to well bore, and it is easier to extract the trapped natural gas. Once the first drill is finished, the isolation plug is inserted, and another well is perforated by firing the perforated gun. With this technique, we can create hundreds of well in this horizontal drilling distance. However, hydraulic fracturing has been well used over 60 years. Hydraulic fracturing is to unlock natural gas out of massive reservoir. The crack initiation has not been understood totally, and the crack network is not understanding for people working in the industries. Thus, this paper is to create a way to understand how the crack network works by using Linear fracture mechanics with boundary element method.

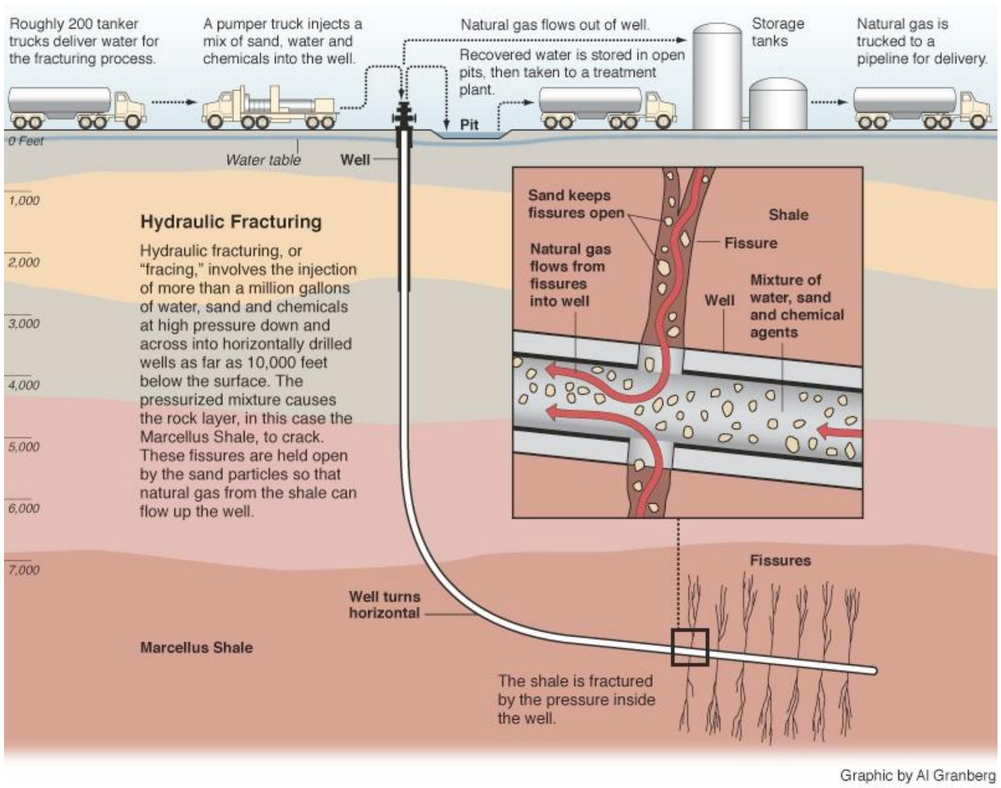

Figure 1 Hydraulic fracturing process in detail graphic by Al Granberg.

1.2 Review Papers

There are plenty of hydraulic fracture studies. Riahi [1] utilized numerical method to study interaction between hydraulic fracture and discrete fracture network with non-polar and polar network in a 2-dimensional case. The objective in this study is to model fluid injection numerically into the fractured rock mass and the discrete fracture network. In this case, we can estimate the hydraulic aperture and Area with respect to time, but we are not able to know how the crack propagates under in-situ stress. Discrete fracture model would be computationally demanding while dealing with sophisticated fractures regarding opening, shearing, or growth, and fluids in the fracture, since discrete fracture model (DFN) treat fractures as entities, but the model did not consider the interaction of hydraulic fractures with pre-existing fractures[2-4]. In addition, a hydraulic fracture will propagate perpendicular to the minimum principal stress. Bai[5] provided a number of injection cases where the important adequate fracture closure and the inadequate case. However, this was not compatible with any plane strain cases of study. Moreover, natural fractures interact with hydraulic fractures under plane strain condition; this can simplify the model into two dimensional cases. A simple test problem with a hydraulic fracture interacting with a natural fracture in a random geometry case was carried out by Jaber [6].The shale gas rock was assumed impermeable, isotropic and elastic. With this, we can know the suituation that hydraulic fracuring interacts with a natural fracture at a certain angle. Jeffery and Zhang [7] propagted that hydraulic aperture was an imaginary opening of closed crack, enabling the aperture to stimulate the residual conductivity of the Nature Fracture (NF) and did not consider the gradient of stress. Chuprakov[8] tried to validate the model on coalescence of fluid flow branches. In the experiment shown in Fig. (1-2), two parallel hydraulic fractures with a 0.8m spcacing were driven by same fluid source, and the natural fracture was going orthogonally with two hydraulic fractures, and the sum of their inflow rates was a constant. They found that the crack continously grew with respect to time when the pressure value met a sufficient value.

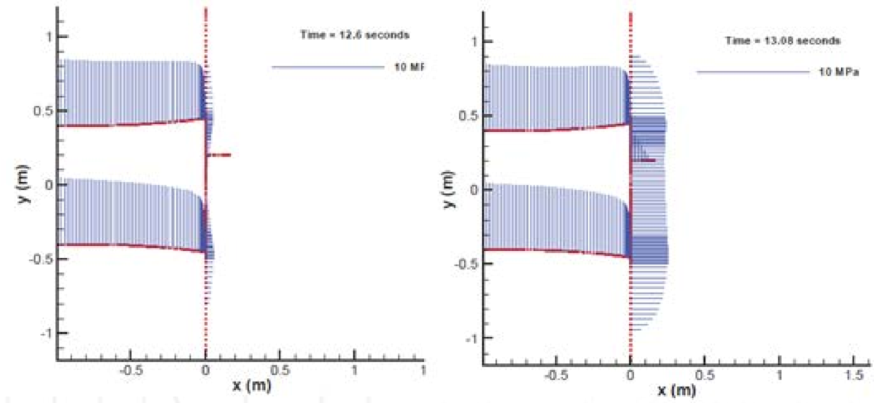

Figure 2 Hydraulic fracturing process in detail graphic by Chuprakov[8].

Chen [9] considered a 2 dimensional hydraulically drvien fracture, propagating in a homogeneous, isotropic, linear elastic, impermeable medium under plane strain conditionby using extended finite element method (XEFM). However, this method was plausible , but it could not tell the whole story for sophisicated crack network. In addition, Jo [10] utilized displacement discontinuity method (DDM) to obtain more accurate Stress Intensity Factor (SIF) in the crack tip and on the fracture profile, and the result of DDM method was compared with other methods, such as analytical method, square root element method, and quarter element method except boundary element method.

1.3 Linear Elastic Fracture Mechanics

Fracture mechanics is the field of study of the formation and propagation of cracks in materials by using analytical solid mechanics to calculate the driving force on a crack and those of experimental solid mechanics to characterize the material's resistance to fracture. Linear elastic fracture assumes the material to be linearly elastic and the crack tip to be sharp. It is applicable to brittle material. In 1920, Griffith [11] observed that larger cracks propagate more easily than smaller ones, he proposed an energy balance criterion to explain the failure of brittle materials. The objective of the theory is to determine whether or not a crack would grow. It states that a crack would propagate if the reduction in strain energy due to its extension exceeds or equals the surface energy increase. In 1956 within the Griffith's energy balance approach, Irwin (ref 13 on page 21 of Anderson's textbook) introduced the concept of energy release rate G as the crack growth driving force. In 1957, he (ref. 15 on page 22 in Anderson's textbook) further introduced the parameter of stress intensity factor KI based on Westergaard's singular stress analysis of a crack in a linearly elastic, isotropic material [12], and related it to the energy release rate. Thus, either the energy release rate or the stress intensity factor maybe be used to rephrase the Griffith fracture criterion: a crack would extend either the energy release rate or the stress intensity factor reaches a threshold, i.e., G >= Gc, or KI >= KIC. This threshold, Gc or K_{IC}, is the critical material resistance to fracture, namely, the material toughness. In the case of linear elastic fracture mechanics (LEFM), the use of stress intensity factors is more convenient, because they can be directly extracted from a stress analysis.

1.4 Boundary Element Method

Boundary element method (BEM) [13] has been popular alongside finite element method (FEM), especially in computational fracture mechanics [14]. Boundary element method is a numerical technique that can be formulated by the reciprocal theorem and by the method of weighted residuals using by Green's function. Compared to FEM, BEM can be often advantageous. BEM would be more accurate than FEM and other numerical methods, since the governing equation is exactly satisfied within the domains. Numerical treatment is only needed upon boundaries and cracks, and solution is more efficient. Moreover, BEM is far more convenient for meshing, etc. We can discretize the boundary alone, and only focus on certain region, which make us engineering work efficiently. Another big advantage of BEM in crack problems over FEM is that domain re-meshing is not necessary when a crack grows; only one more element is possible if a crack is added with the already existing elements un-interacted.

1.5 Rock Mechanics

Shale gas is natural gas trapped in low-permeability shale rocks. From those low permeability and heterogeneity characteristics, the mass formation of shale gas happens in the Earth Crust. This sedimentary rock has been strengthened during geological evolution. In the following, we review some previous papers with pertinent material properties and typical values of pressure in hydraulic fracturing. In our present study, we need to know the range of K_{IC} and the range of loading pressure.

From Chuprakov [15] to study fracture propagation across a weak discontinuity, Chuprakov used K_{IC} in the range from 0.1 to $2.7 MPa \cdot m^{0.5}$, as shown below

Table 1 Range of the problem's dimensional specific to gas shale fracturing jobs.

Parameter		Range
Q	Volumetric injection rate	0.01–0.25 m^3/s mmoposdvrgenmk m^3/sec
L	Distance between HF and NF	1–10 m
μ	Fluid viscosity	1–1000 cP
E	Young's modulus	9–110 GPa
v	Poisson's coefficient	0.11 –0.252
K_{IC}	Mode I fracture toughness	0.1–2.7 MPa($m^{1/2}$)
$K_{IC}^{(NF)}/K_{IC}^{(RM)}$	Toughness ratio for NF vs. rock matrix	0–0.5
$K_{IC}^{(NF)}/K_{IC}^{(NF)}$	Toughness ratio for NF	~1
σ_1	Maximum in-situ stress	13–105 MPa
σ_2	Minimum in-situ stress	11–100 MPa
λ	Friction coefficient at the NF	0.2–1
k_n	Permeability of NF	1 md–1 darcy
β	Fracture interaction angles	30°–90°

Kear[16] provided in CSRO commercial software, and K_{IC} was 2.3 Mpa.$m^{0.5}$, shown in the below chart.

Table 2 Adelaide Black Granite material properties.

Fracture toughness	K_{Ic}	2.3 MPa.m$^{0.5}$
Young's modulus	E	102 GPa
Poisson's Ratio	v	0.27
Tensile Strength	TS	9.4 MPa
Friction coefficient	f	0.45 (coarse finish) to 0.17 (polished finish)
Crystal Size		1-10mm diameter (typical)

The chart below was provided by Adams[17]. Adams intended to find a more reasonable hydraulic pumping pressure. He applied more than 15K psi to extract oil and gas out of tight reservoirs, as shown in the following figure.

Table 3 Treatments based on conventional oil and gas method.

	Volume (L)					Frac
O&G Tight Reservoirs	10^6	Yes	Yes	Up to 15K psi	Yes	Yes
Water Wells	$<10^3$	No	Some	<3,000 psi	Yes	Few
Block Cave Mining	10^4	No	Some	<10K psi	<100m	Yes
Rock Stress Testing	$<10^3$	No	No	<15K psi	Limited	Yes
Conventional Oil & Gas	10^6	Yes	Yes	Up to 15K psi	Yes	Yes
Enhanced Geothermal	10^7	Yes	Yes	Up to 15K psi	Yes	Yes
Carbon sequestration	10^6	Yes	Yes	Up to 10K psi	Yes	Yes
CBM	$<5x10^5$	Some	Yes	<5Kpsi	Yes	Yes
CMM	10^4	Some	Some	<5Kpsi	Yes	Yes
Rock Burst Mitigation	$<10^3$	No	No	<15K psi	Limited	Yes

Kresse[18] studied the flow rate and the viscosity of the fluid, which is not used in our present study but may be useful for future further study, as shown in the following chart.

Table 4 Input data for Barnett Shale case.

Parameters	Xlink Gel treatment	Slick Water treatment
Young's modulus	4.8×10^6 psi	
Natural fracture direction	Average N70°W, standard deviation 5°	
Natural fracture length	Average 200 ft, standard deviation 40 ft	
Natural fracture spacing	Average 100 ft, standard deviation 20 ft	
Coefficient of friction	Average 0.6, standard deviation 0.1	
Hydraulic fracture direction	N40°E	
Minimum horizontal stress	5324 psi	
Maximum horizontal stress	5524 psi	
Fracture height	310 ft	360 ft
Fluid rheology	$n' = 0.42$, $k' = 0.002$ lb-s/ft^2	1 cp
Injection rate : Q	70 bpm	125 bpm
Pump time	174 min	386 min
Proppant volume	715,000 lbs	600,000 lbs

Men[19] used fracture toughness to simulate hydraulic fracturing in heterogeneous rock, which is a good reference for our present research. The two figures are shown below.

Table 5 Rock material mechanical parameter

Parameter	Symbol	Value
Homogeneity index	m	2
Elastic modulus	E_c	30 GPa
Poisson's ratio	μ	0.25
Internal friction angle	ϕ	37
Uniaxial compressive strength	f_c	200 MPa
Coefficient of permeability	K	0.000864 m/d

Table 6 Bedding material mechanical parameter.

Parameter	Symbol	Value
Homogeneity index	m	2
Elastic modulus	E_c	3.0 GPa
Poisson's ratio	μ	0.25
Internal friction angle	ϕ	37
Uniaxial compressive strength	f_c	20 MPa
Coefficient of permeability	K	0.00864 m/d

Table 7 Change of elastic modulus and uniaxial compressive strength values of bedding material.

Rock material		Bedding material	
Elastic modulus (E_c)	Uniaxial compressive strength (f_c)	Elastic modulus (E_c)	Uniaxial compressive strength (f_c)
30GPa	200MPa	3.0GPa(1/10)	200MPa(1)
30GPa	200MPa	1.5GPa(1/20)	200MPa(1)
30GPa	200MPa	0.5GPa(1/60)	200MPa(1)
30GPa	200MPa	30GPa(1)	20MPa(1/10)
30GPa	200MPa	30GPa(1)	10MPa(1/20)
30GPa	200MPa	30GPa(1)	3.33MPa(1/60)
30GPa	200MPa	3.0GPa(1/10)	20MPa(1/10)

Sesetty[20] simulated sequential and simultaneous hydraulic fracturing, with a two dimensional coupled displacement discontinuity numerical model for crack propagation. The parameters used in this study are shown below.

Table 8 Input data in displacement discontinuity numerical model

Parameter	Value	Units
Young's modulus	27	GPa
Poisson's ratio	0.25	
$\sigma_{H/}$ σ_h (Max/Min In-situ horizontal stress)	5/4	MPa
Injection rate (stage-1)/(stage-2)	20/40	bpm
Viscosity	1	cP
Fracture height	30	ft
Fracture toughness	2	$MPa.m^{1/2}$

Zhang [21] in Discrete Fracture Network model used parameters with maximum horizontal stress equal to 55MPa, and minimum horizontal stress equal to 50 MPa. On the other hand, the vertical stress was 60 MPa.

Chapter 2

Problem Formation

In conventional reservoirs, pumping is the easiest way to extract the oil and gas. In contrast, in unconventional shale gas reservoirs, hydraulic fracturing is used to extract the shale gas. Since the shale is a low permeability sedimentary rock with natural cracks, each well is perforated by firing the perforated gun, which initiates the cracks orthogonal to the main well by thousands of miles. By hundreds of hydraulic fracturing, the sophisticated hydraulic fractured crack network is created. Since the pressure (traction) in normal direction is under compression along the thickness direction of shale gas rock, we can simplify into plain strain condition. As a result, the model could be simplified into a two-dimensional case. In the present study, we use boundary element method to simulate growing cracks in order to better understand the interaction between new and pre-existing cracks to see if the cracks would arrest, promote, or bifurcate each other. Boundary element method can provide us an analytical method to understand the crack initiation and propagation. LEFM is the fundamental theory we use to characterize the cracks in rocks.

2.1 Basic Equations of Elasticity

Let us consider a homogeneous, isotropic, linearly elastic domain Ω of piecewise smooth boundary Γ, as shown in Fig. 2.1. The equilibrium equations at a point xϵΩ, in absence of inertia effects, are

$$\sigma_{ij,j} + bi = 0, \qquad (2.1)$$

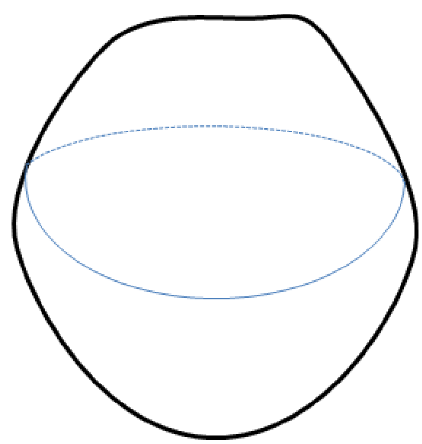

Figure 3 A homogenous, isotropic, linearly elastic body Ω with piecewise smooth boundary Γ in equilibrium.

Where σij are components of the stress tensor, bi is the body force per unit volume, and ,j is partial differentiation with respect to xj. The indices I and j range from 1 to 3, which refer to Cartesian coordinate directions. When an index in a subscript is repeated in any particular term, a summation over that index is implied. However, the convention of summation is not applicable to superscript indices. When describing two-dimensional problems, Greek indices may be utilized instead, ranging from 1 to 2. The stress-displacement relationships are

$$\sigma_{ij} = \lambda\delta_{ij}u_{k,k} + \mu(u_{i,j} + u_{j,i}), \quad (2.2)$$

Where λ and μ are the Lame's constants which are related to Young modulus E and Poisson's ratio ν by

$$\lambda = \frac{\nu E}{(1+\nu)(1-2\nu)} \quad (2.3)$$

$$\mu = \frac{E}{2(1+\nu)} \quad (2.4)$$

In the above equations (2.3) and (2.4) , σ_{ij} is the Kronecker delta which equals to 1 if i = j, and 0 otherwise. By substituting Eq. (2.2) into Eq. (2.1), we can obtain Navier's equations,

$$(\lambda + \mu)uk,ki + \mu\, ui,kk + bi = 0, \quad (2.5)$$

Proper boundary conditions along boundary Γ is imposed in order to have unique solutions to Eq. (2.5). If either displacements ui or traction pi (= σijnj) are given for any boundary point,

$u_i = u_i$ or $p_i = p_i$,

nj is outward normal vector at a boundary point. However, in some cases, the formulation of the boundary creates a problem must be adjusted.

Then consider a body **Ω** with external boundary Γex and singular surfaces Γc across which a displacement jump occurs, as shown in Fig. 2.2. The stress and displacement relationship in the bulk material is assumed to be the same as given by Eq. (2.2). The whole domain satisfies equilibrium condition Eq. (2.1). External boundary Γex was using the boundary condition given by Eq. (2.6), and the following relationship is used to relate traction p with the displacement jump w across the singular surfaces Γc,

$P_{i=}f_i(w)$ on Γ^c, with $w=u^- - u^+$ (2.7)

Where fi is a given function, u- and u+ are the displacements on either sides of the singular surfaces. The singular surfaces may be in contact or opening. If fi is identical to zero, which are traction-free crack in the singular surfaces, the stress field around the crack tip is singular. The singularity- based model will be discussed in Section 2.2. If fi is not trivial, it can induce to cohesive zone model of a crack; with the non-trivial traction, the singularity term in stress field at the crack tip will be eliminated. The cohesive zone will not be discussed in this study. In the contact mode, Eqs.(2.7) is proper to describe the behavior of the tangential interaction of the singular surfaces. The contact mode of the singular surfaces will be described in Section 2.4. We now turn to the description of the singular crack-tip stress field for the opening traction-free cracks.

2.2 Singularity-based Fracture Mechanics (L.E.F.M.)

Consider a mathematical planar traction-free sharp crack tip in linear elasticity under far-field loading maybe expressed as

$$\sigma_{ij} = \left(\frac{k}{\sqrt{r}}\right) f_{ij}(\theta) + \sum_{m=0}^{\infty} A_m r_{\sigma_{yy}}^{\frac{m}{2}} g_{ij}{}^{m}(\theta) \qquad (2.8)$$

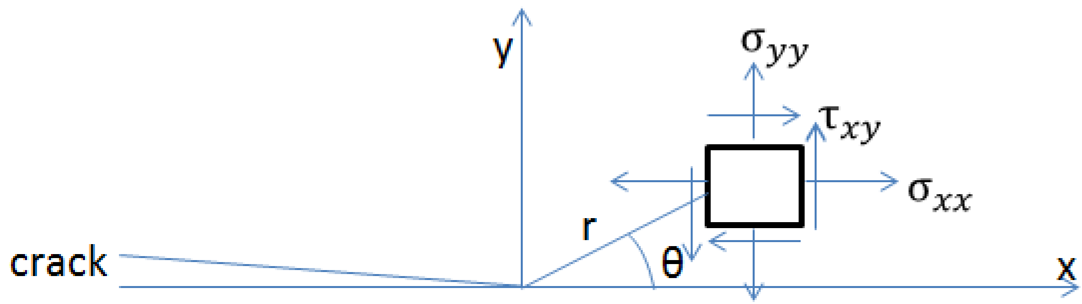

Figure 4 Stress field at crack tip in linear elasticity.

Where k and A_m are all constants to be determined by loading conditions. The complicated loading condition can be differentiated into three modes: opening mode (mode I), in-plane shear (mode II), and out-of-plane shear (mode III). There is a singularity at r-1/2 in the Williams' expansion. First, in mode I, the forces are perpendicular to the crack pulling the crack open. The crack is horizontal and the forces are vertical. Second, in mode II, the forces are parallel to the crack. Basically, one is pulling the top half of the crack forward, and the other is pulling the bottom half of the crack backward. The crack is sliding along itself. In plane shear is that the forces are causing the material moves along the crack plane. Third, mode III is called out of plane shear. The forces are perpendicular to the crack, and move in the front and back direction. This causes the material to separate and move out of the original plane. Stress intensity factor KI, KII, and KIII are used to characterize energy release rate of the fields, which is independent to specimen geometry, loading condition, and environment. The equations show in Eqs (2-9) and (2-10) KI, KII, and KIII in mode I and mode II in Cartesian coordinaters (x1, x2) and polar coordinates (r, θ)

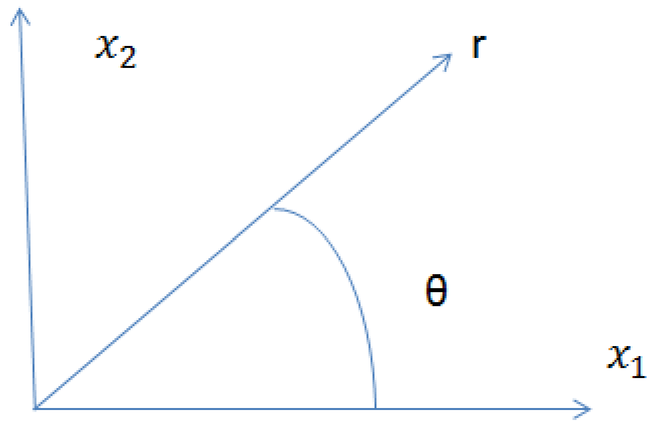

Figure 5 A mathematical planar crack in Cartesian coordinates (x1, x2) and polar coordinates

$$\begin{pmatrix} \sigma_{11} \\ \sigma_{12} \\ \sigma_{22} \end{pmatrix} = \frac{K_I}{(2\pi r)^{1/2}} \cos\left(\frac{\theta}{2}\right) \begin{pmatrix} 1-\sin\left(\frac{\theta}{2}\right)\sin\left(\frac{3\theta}{2}\right) \\ \sin\left(\frac{\theta}{2}\right)\cos\left(\frac{3\theta}{2}\right) \\ 1+\sin\left(\frac{\theta}{2}\right)\sin\left(\frac{3\theta}{2}\right) \end{pmatrix} + \begin{pmatrix} T \\ 0 \\ 0 \end{pmatrix} + 0\,(r^{1/2}) \qquad (2\text{-}9)$$

$$\begin{pmatrix} \sigma_{11} \\ \sigma_{12} \\ \sigma_{22} \end{pmatrix} = \frac{K_{II}}{(2\pi r)^{1/2}} \begin{pmatrix} -\sin\left(\frac{\theta}{2}\right)\left[2+\cos\left(\frac{\theta}{2}\right)\cos\left(\frac{3\theta}{2}\right)\right] \\ \cos\left(\frac{\theta}{2}\right)\left[1-\sin\left(\frac{\theta}{2}\right)\sin\left(\frac{3\theta}{2}\right)\right] \\ \sin\left(\frac{\theta}{2}\right)\cos\left(\frac{\theta}{2}\right)\cos\left(\frac{3\theta}{2}\right) \end{pmatrix} + 0\,(r^{1/2}) \qquad (2\text{-}10)$$

Where μ is the shear modulus, κ is (3-4ν) on plane strain condition, and κ is (3-ν)/(1+ ν) on plane stress condition.

2.3 Crack Initiation and Propagation Criteria

Strength and dissipation capacity are two key materials properties to crack initiation and propagation analyses. When the stress at a crack tip reaches the strength, the crack starts to develop a fracture process zone without crack propagation. The crack grows after the process zone is fully developed or the structure has become structurally unstable. During the crack propagation, the crack tip advances along with the process zone tip. There are a few criteria for crack initiation and propagation in brittle materials proposed in the literature, which take into account the dissipation energy only, as discussed before in Griffith's theory[11]. We utilize the maximum tangential stress (MTS) criterion in the framework of LEFM. Based on in Yang's paper[22], the T-stress and other higher-order terms of the crack-tip stress field have no direct effect in determining crack path in this approach because of the singularity dominance.

2.4 MTS Criterion in LEFM

In the polar coordinates, the tangential component of the two-dimensional in-plane asymptotic stress field can be presented by

$$\sigma_\theta = \frac{1}{\sqrt{2\pi \mathrm{r}}} cos^2\left(\frac{\theta}{2}\right)\left(K_I \cos(\frac{\theta}{2}) - 3K_{II} \sin(\frac{\theta}{2})\right) \tag{2.11}$$

The maximum tangential stress can be achieved in the direction.

$$\theta_I = 2\tan^{-1}\left\{\frac{K_I - \sqrt{{K_I}^2 + 8{K_{II}}^2}}{4K_{II}}\right\}, \tag{2.12}$$

by solving the equation of the first derivative of stress with respect to θ equal to zero, which means the stationary points, and under the condition of the second derivative of stress with respect to theta being negative in Yang's study[23], which means the slope concaving down. Substituting Eq. (2.12) into Eq. (2.11), the effective mode-I stress intensity factor along the direction of MTS is obtained,

$$k_I = \sigma_{\theta I}\sqrt{2\pi \mathrm{r}} = \frac{K_I}{2\mu} K_I cos^3\left(\frac{\theta_I}{2}\right) - 3K_{II}\sin(\frac{\theta_I}{2})cos^2(\frac{\theta_I}{2}) \qquad (2.13)$$

The MTS criterion states that a crack grows when KI is larger than fracture toughness (KIC), i.e.,

$$k_I \geq K_{IC}, \qquad (2.14)$$

$\mathrm{K_{IC}}$ is a material constant to be acquired by experiments.

We should be aware of that the maximum tangential stress derived above is not the maximum tensile stress that happens in the crack tip region. The MTS is not a criterion of material strength, but a criterion of energy release rate. In fact, Nuismer [24] (1975) proved that MTS is a equivalent to the maximum energy release rate criterion based on energy consideration.

Chapter 3

Boundary Element Method

3.1 The Single Domain Dual Integral Equations for a Cracked Structure

In this section, a structure containing a mathematically sharp crack degenerates the boundary integral formulation because of coincidence of the crack surfaces. Based on Yang's study[25], we can use a single-domain dual-boundary-integral method to approach this problem. The formulation of a single-domain dual-boundary-integral method is based on Kelvin's solutions. In order to apply the dual integral equation to each separated domain, we cut a domain with crack elastostatic structure into subdomains of simple topology. As shown in Figure 3-1, a structure with a crack can be sect into two subdomains with a path that circulate into each subdomain. First, the value of the external regular boundary should equal to the sum of two sub-domains' integral values. Second, we apply continuity condition at displacement components at the points along the artificial boundary, and we can set the displacement components in two sub-domains are the same. Third, we set traction components in two sub-domains are equal magnitude but opposite direction due to structure equilibrium. Fourth, the integral kernels are the same magnitude but in opposite values. Applying all conditions we mentioned above, we also neglect the body force term for simplicity. We can obtain the well-known single-domain dual integral equations of a cracked structure in Eqs. (3-1) and (3-3).

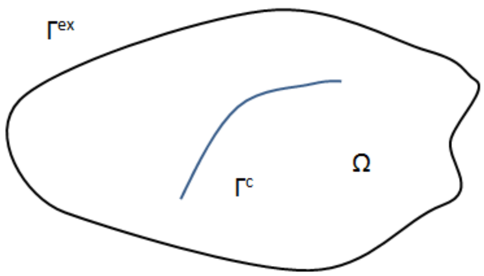

Figure 6 A domain Ω with a crack Γc.

$$I_i(x) = \int_{\Gamma^{ex}} \{u^*_{ij}(X,x)p_j(X) - p^*_{ij}(X,x,n)u_j(x)\}d\Gamma(x) + \int_{\Gamma^c}\{u^*_{ij}(X,x)\left[p^+_j(X) + p^-_j(X)\right] - \left[p^*_{ij}(X,x,n^+)(u^+_j(x) - u^-_j(x))\right]\right\} d\Gamma(x) \quad (3.1)$$

with

$$I_i(x) = \begin{cases} u_i(X) & X\epsilon\,\Omega\,; \\ c_{ij}(X)u_i(X) & X\epsilon\,\Gamma^{ex}\,; \\ c^+_{ij}(X)u^+_j(X) + c^-_{ij}(X)u^-_j(X) & X\epsilon\,\Gamma^c\,; \\ 0 & otherwise, \end{cases} \quad (3.2)$$

and

$$J_{ij}(X) = \int_{\Gamma^{ex}}\{U^*_{ijk}(X,x)p_k(x) - p^*_{ijk}(X,x,n)u_k(x)\}d\Gamma(x) + \int_{\Gamma^c}\{u^*_{ijk}(X,x)[p^+_k(x) + p^-_k(x)] - \left[P^*_{ijk}(X,x,n^+)\left(u^+_k(x) - u^-_k(x)\right)\right]\right\} d\Gamma(x), \quad (3.3)$$

with

$$J_{ij}(X) = \begin{cases} \sigma_{ij}(X) & X \epsilon\, \Omega\,; \\ \sigma_{ij}(X)\,/2 & X \epsilon\, \Gamma^{ex}; \\ \left(\sigma_{ij}^{+}(X) + \sigma_{ij}^{-}(X)\right)/2 & X \epsilon\, \Gamma^{c}; \\ 0 & otherwise, \end{cases} \qquad (3.4)$$

Where, the superscript + is a side of a crack, and the superscript – is the corresponding opposite side. The positive side of rack can be chosen arbitrarily. Regarding a crack problem, we can use the integrals along the regular external boundary and one side of a crack. For multiple cracks, we can create several sub-domains to solve the problem by using the same concept. The equation is given in the same forms as Eqs. (3-1) and (3-2).

Eqs. (3-1) and (3-2) with a source point on the boundary, i.e., $X \in \Gamma^{ex+c}$, are of the most importance, in the formulation of boundary integral equations of elastostatic problems. If they are “multiplied” on the both sides by the outward normal at the boundary point X on Eqs. (3-3) with the boundary at $X \in \Gamma^{ex+c}$, we obtain

$$J_{ij}(X)n_j(X) =$$

$$\int_{\Gamma^{ex}}\{U_{ijk}^{*}(X,x)p_k(x) - p_{ijk}^{*}(X,x,n)u_k(x)\}d\Gamma(x) + \int_{\Gamma^{c}}\{U_{ijk}^{*}(X,x)[p_k^{+}(x) +$$

$$p_k^{-}(x)] - \left[P_{ijk}^{*}(X,x,n^{+})\left(u_k^{+}(x) - u_k^{-}(x)\right)\right]\}n_j(X)d\Gamma(x). \qquad (3.5)$$

Where $n_j(x)$ is taken to be the outward normal of the positive crack side. On the crack surfaces, the tractions are self-equilibrating and hence

$$\frac{n_j^{+}(X)\left(\sigma_{ij}^{+}(X)+\sigma_{ij}^{-}(X)\right)}{2} = p_i^{+}(X) \quad \text{and} \quad p_i^{+}(X) + p_i^{-}(X) = 0. \qquad (3.6)$$

In this case, traction and displacement on a crack jump can be treated as independent variables in a numerical formulation.

3.2 Numerical Implementation

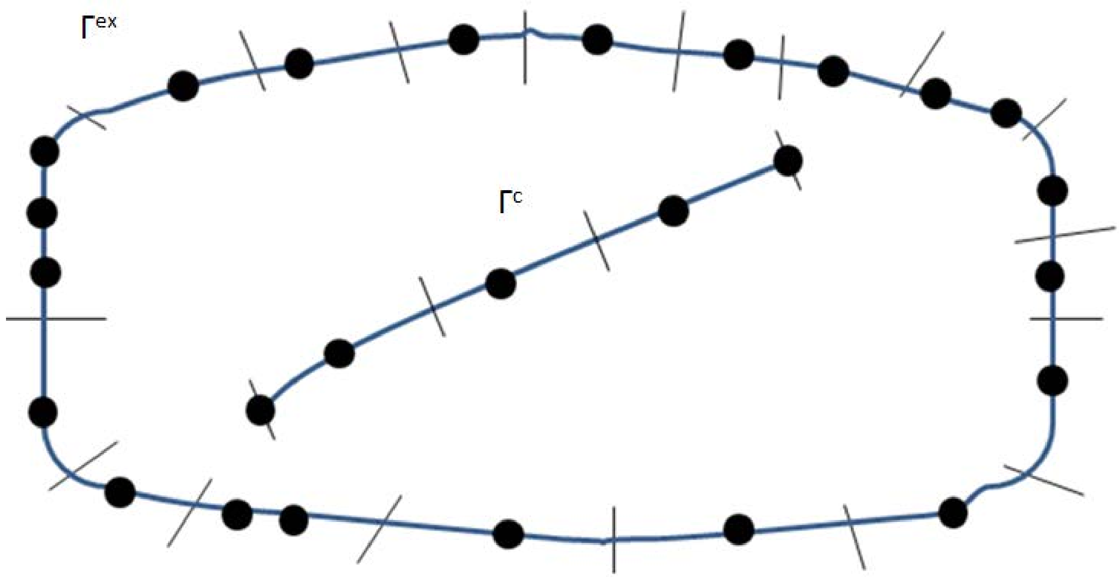

Figure 7 The discretization of the boundary into elements is shown in this figure. One or more nodes are evenly distributed in each element. The nodes are external to the element, indicating discontinuous elements.

The boundaries of a cracked two dimensional structure is discretized into straight elements, Γel, with distributed nodes, Nel in each element, as shown in figure 3-2 We assume that we have Nex nodes on the external boundary, and Nc nodes on the crack locus. A field quantity can be approximated through an element Γ_{el} by interpolating the nodal values, qn in this element, we obtain

$$q(x) = \sum_{n=1}^{N^{el}} \phi^n(x)\phi q^n \tag{3.7}$$

The discretized forms of the dual boundary integral equations can be obtained.

$$\sum_{n=1}^{N^{el}} (g_{\alpha\beta}^{mn} p_\beta^n - h_{\alpha\beta}^{mn} u_\beta^n) + \sum_{n=N^{ex}+1}^{N^{ex}+N^c} h_{\alpha\beta}^{mn} w_\beta^n - I_\alpha(X^m) = 0, \tag{3.8}$$

And

$$\sum_{n=1}^{N^{el}} (G_{\alpha\beta}^{mn} p_\beta^n - H_{\alpha\beta}^{mn} u_\beta^n) + \sum_{n=N^{ex}+1}^{N^{ex}+N^c} H_{\alpha\beta}^{mn} w_\beta^n - J_{\alpha\beta}(X^m) n_\beta(X^m) = 0, m = 1,2,, \ldots N^{ex} + N^c. \tag{3.9}$$

Eqs. (3.8) and (3.9) each represent $2(N^{ex}+N^c)$ equations that are discretized version of Eqs. (3.1) and (3.4). We can obtain $g_{\alpha\beta}^{mn}$, $h_{\alpha\beta}^{mn}$, $G_{\alpha\beta}^{mn}$, $H_{\alpha\beta}^{mn}$ are given separately below, where Γ^n is the element where the nth node is located.

$$g_{\alpha\beta}^{mn} = \int_{\Gamma^n} u_{\alpha\beta}^* (X^m, x)\phi^n(x) d\Gamma(x), \tag{3.10}$$

$$h_{\alpha\beta}^{mn} = \int_{\Gamma^n} p_{\alpha\beta}^* (X^m, x)\phi^n(x) d\Gamma(x), \tag{3.11}$$

$$G_{\alpha\beta}^{mn} = \int_{\Gamma^n} U_{\alpha\delta\beta}^* (X^m, x)\phi^n(x) n_\delta(X^m) d\Gamma(x), \tag{3.12}$$

$$H_{\alpha\beta}^{mn} = \int_{\Gamma^n} u_{\alpha\delta\beta}^* (X^m, x, n)\phi^n(x) n_\delta(X^m) d\Gamma(x), \tag{3.13}$$

Where Γ^n is the element where the nth node is located. Eqs. (3.10) thru Eqs. (3.13) may be evaluated numerically if $X^m \notin \Gamma^n$, and analytically if $X^m \in \Gamma^n$. Note that the condition for a self-equilibrating crack, Eqs. (3.6), has been utilized in the above equations.

If u and p are different displacement and traction from the exact solution, Eqs. (3.8) and Eqs. (3.9) would not be satisfied, leaving residuals:

$$r_\alpha^m(u,p) = \sum_{n=1}^{N^{ex}}\left(g_{\alpha\beta}^{mn} p_\beta^n - h_{\alpha\beta}^{mn} u_\beta^n\right) + \sum_{n=N^{ex}+1}^{N^{ex}+N^c} h_{\alpha\beta}^{mn} w_\beta^n - I_\alpha(X^m) = 0, m = 1,2,,\ldots N^{ex} + N^c, \tag{3.14}$$

$$R_\alpha^m(u,p) = \sum_{n=1}^{N^{ex}}\left(G_{\alpha\beta}^{mn} p_\beta^n - H_{\alpha\beta}^{mn} u_\beta^n\right) + \sum_{n=N^{ex}+1}^{N^{ex}+N^c} H_{\alpha\beta}^{mn} w_\beta^n - J_{\alpha\beta}(X^m) n_\beta(X^m) = 0, m = 1,2,,\ldots N^{ex} + N^c, \tag{3.15}$$

We state the displacement residual, r_α^m and the traction residual, R_α^m. If the residuals are close to zero, the values of u and p represent an approximate solution of the boundary value problem. Either displacement or traction vector components can be prescribed at all regular boundary points, and the other will be induced. In order to handle crack sliding and crack contact modes of deformation, field quantities in the discretized equations must be transformed into the local orthogonal coordinates in term of the normal and tangential directions.

In the iterative solution scheme, a quantity $q_\alpha^{(m,l+1)}$ at the (l+1)th iteration isobtained from the value at the lth iteration, $q_\alpha^{m,l}$, and The increment is given by

$$q_\alpha^{m,l+1} = q_\alpha^{m,l} - \frac{R}{\frac{\partial R}{\partial q_\alpha^m}}\Big|^{l} \tag{3.16}$$

Where R is the appropriate residual for the field quantity q_α^m at the lth iteration. In addition, the displacement component $u_\alpha^{m,l+1}$ is at (l+1)th iteration step.

$$u_{\alpha}^{m,l+1}=u_{\alpha}^{m,l}+\frac{\omega r_{\alpha}^{m,l}\left(u,p\right)}{(c_{\alpha\alpha}^{m}+h_{\alpha\alpha}^{mm})}\text{, (no sum on }\alpha\text{)} \tag{3.17}$$

Where w is an adjustable factor of relaxation. The displacement residual, $r_{\alpha}^{m}\left(u,p\right)$, is calculated by using the nodal values at the (l+1)th iteration step if available or 1th iteration. Similarly, a traction component $p_{\alpha}^{m,l+1}$, is calculated by using the results at the lth iteration by

$$p_{\alpha}^{m,l+1}=p_{\alpha}^{m,}+\omega R_{\alpha}^{m}\left(u,p\right)/\left(0.5\text{-}G_{\alpha\alpha}^{mm}\right)\text{, (no sum on }\alpha\text{)} \tag{3.18}$$

Where the traction residual, $R_{\alpha}^{m}\left(u,p\right)$, is calculated by using the nodal values at the (l+1)th iteration step if available or 1th iteration, and node m is on the boundary, and then we obtain the displacement discontinuity,

$$w_{\alpha}^{m,l+1}=w_{\alpha}^{m,l}+v\left(u,p\right)/\left(k^{m,l}\text{-}H_{\alpha\alpha}^{mm}\right)\text{ , (no sum on }\alpha\text{)} \tag{3.19}$$

Where ϖ is another adjustable relaxation.

The numerical solution in the boundary element method is obtained in three main steps. First, suppose that the solution at the previous load step is known. In order to solve the problems in the current step, the crack body is iterated to be in equilibrium with all the current nodes being held at the same displacement by using Eqs. (3.17) and (3.18). Second, the crack tip has been fixed at this step for the purpose to not grow cracks in this step. The whole body is to maintain equilibrium by using Eqs. (3.17) until (3.19). This holding and releasing process is to produce efficient convergence for the iteration process when cracks propagate. The absolute difference of either displacement or traction between two successive iteration steps can be used to judge for the convergence. The best relaxation factor mostly depends on geometry shape and the loading conditions. In the third steps, stresses at a point of the crack tip are obtained by extrapolation of the stresses at three close points by using Eqs. (3.18). The crack will propagate when the effective KI is greater than KIC. The crack tip will propagate in a small increment in the direction determined by M.T.S criterion.

Chapter 4

Linear Elastic Fracture Mechanics Stimulation

In this study, we stimulate a hydraulic fracturing with loading condition under plane strain condition; we can simplify this problem as two dimensional. The driving force is the hydraulic pumping pressure. The determining parameters in this study are normalized K_{IC}, and p, pressure in the direction normal to the wells. These two key parameters are described below:

$$\overline{K_{IC}} = \frac{K_{IC}}{E\sqrt{b}} \qquad (4\text{-}1)$$

Where b is characteristic length scale, taken as the pressure zone size, K_{IC} is the fracture toughness of shale rock, and E is Young's modulus of shale rock.

$$\bar{P} = \frac{P}{E} \qquad (4\text{-}2)$$

where P is applied over the pressure zone and over the crack sides connected to the pressure zone, and E is Young's modulus of shale rock. With these properties, we can simulate a practical case. The values K_{IC} = 2.3 MPa.m$^{0.5}$, Young Modulus E = 25 GPa from Hay [26].In addition, pumping pressure is set to be 0.103GPa, a typical value used by some big oil companies. Based on Eqs. (4-1) and (4-2), we obtained our normalized P = 0.00412, normalized K_{IC} =0.0001, with b =1 m.

First, we take 5 cracks, and try to grow them in multiple steps under a constant hydraulic pressure. Based on the crack propagation criterion in LEFM, if $K_I > K_{IC}$, cracks propagate. From Figure 4-1 we fix the bottom side, and on the top side we apply an evenly distributed load in our two dimensional model. It is observed that the cracks are closed if they are beneath the pressure zone. However, the cracks may experience a mode-II shear loading. They can kink to obtain opening mode driving force according to the MTS criterion. This driving force may sustain the cracks to grow in opening mode for a short distance and then vanishes. At that point, the crack is closed again; it would remain dormant unless further loading is applied. For instance, the two in-between cracks (# 2 and # 4) kink out due to KII dominated loading, as shown in Figure 4-2. The value in KI is about zero and the value in KII is 0.00015. As a result, the cracks are under shearing at the first step. Crack # 1 and crack # 5 are not directly under the pressure zone, and grow successfully. At first step, the values of KI and KII are close, as shown in Figure 4-1 and Figure 4-2. The first step is where the crack kink out with mixed shearing and opening modes. After that step, the value of KI is all greater than KII. The effective KI is slightly greater than KI, as shown in Figure 4-1 and Figure 4-3, indicating that there is a small KII along its path. It keeps driving the cracks to modify its growth direction. The effective KII is always equal to zero as a consequence of the MTS criterion.

With this example, we checked the convergence of solution with crack advance step. The results of KI for two different advance steps = 0.05 and = 0.08 are shown in Figure 4-5. It can be seen that the difference due to the different values of advance step is negligible, demonstrating the convergence in our numerical calculation. Thus, the results presented herein are reliable.

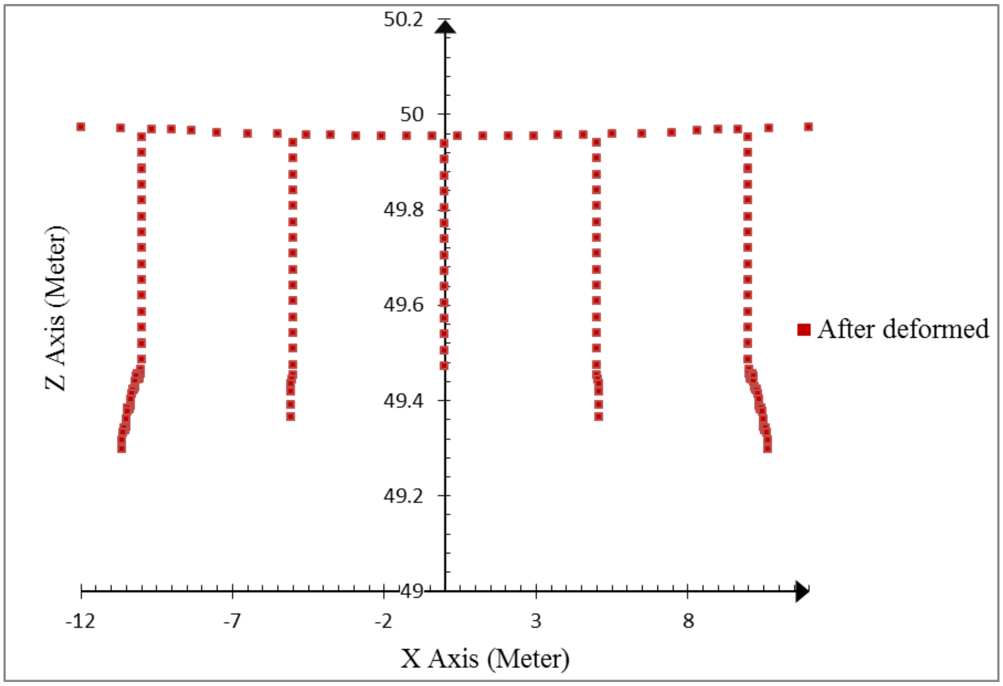

Figure 8 A set of crack pressurized at the domain between -8 to 8 in 10 steps with accelerate crack growth at 0.08 after deformed.

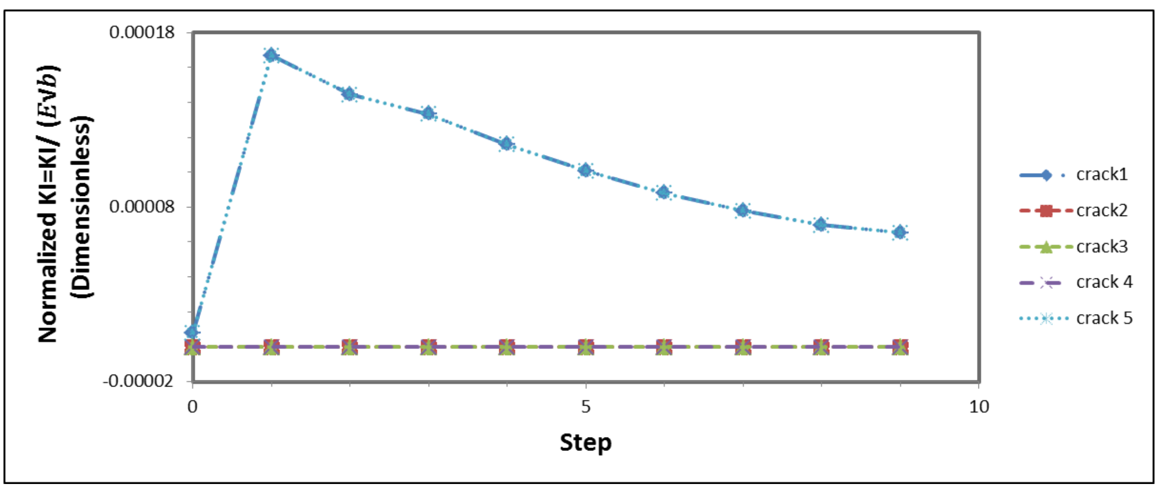

Figure 9 K1 in cracks in 10 steps with accelerate crack growth at 0.08, series 1 to 5 is from left to right crack.

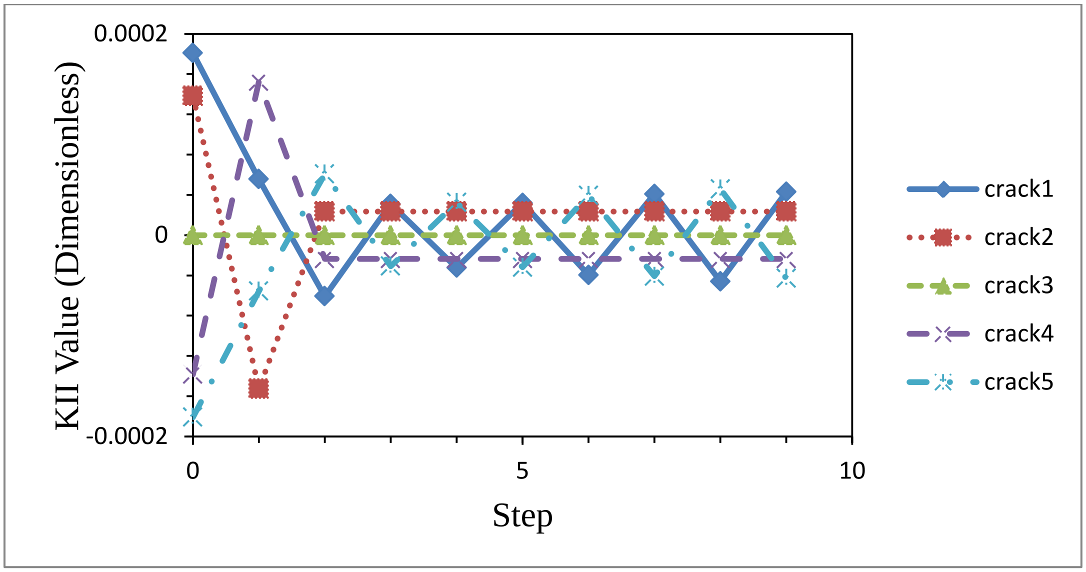

Figure 10 KII in cracks in 10 steps with accelerate crack growth at 0.08, series 1 to 5 is from left to right crack.

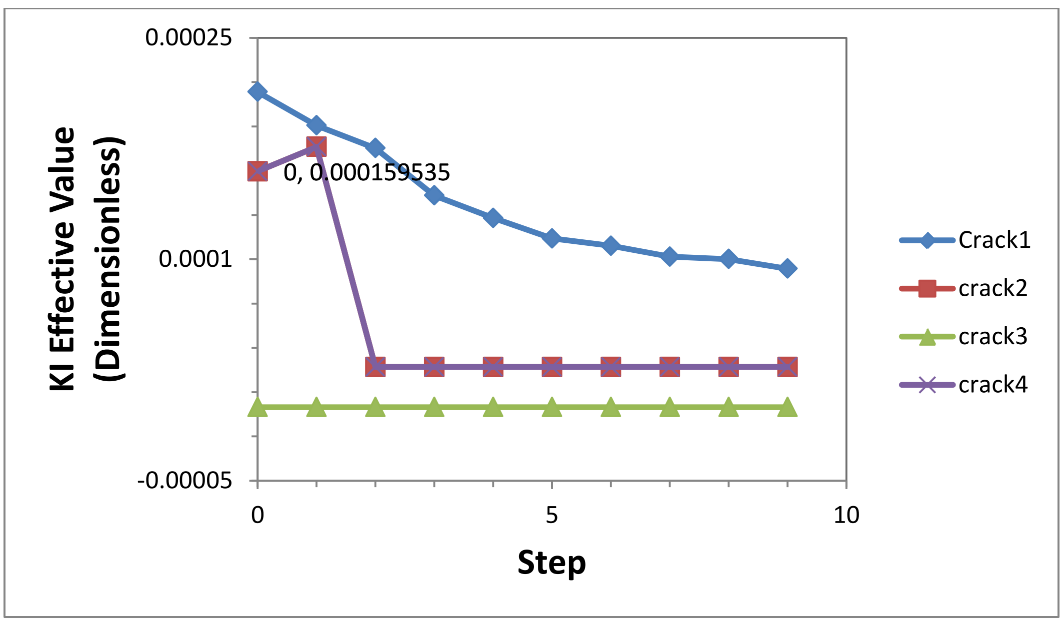

Figure 11 K1 effective in cracks in 10 steps with accelerate crack growth at 0.08, crack to 5 is from left to right crack.

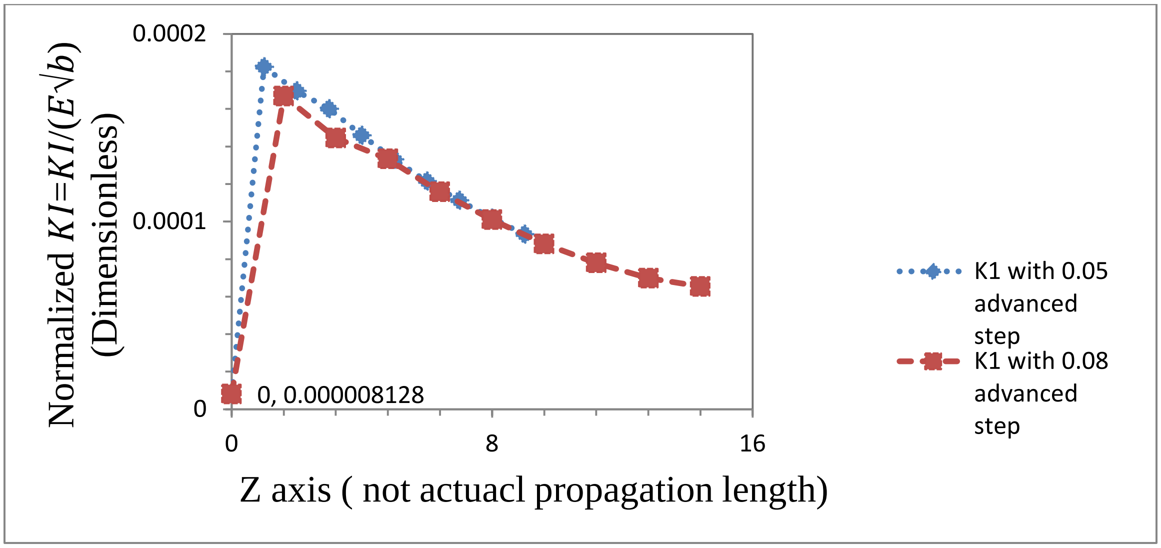

Figure 12 KI advanced 0.05 and KI advanced 0.08. Series1 is 0.05 advanced step and Series2 is 0.05 advanced step.

Second, we consider a case with 10 cracks, two sets each of 5 cracks beside a pressured zone in the middle on the top surface, as shown in Figure 4-6. The pressured space is from -10 to 10. We found that the outside cracks would propagate with a greater driving force than those inside ones. The two most inner cracks (crack #5 and crack#6) at the edges of loading kink out under mixed KI and KII with KII dominating, as shown in Figure 4-7 and Figure 4-8. Crack#4 and crack#7 were mainly arrested and closed. Crack (# 1, # 2, and # 3) and Crack (# 8, # 9, and # 10) will depend on the ratio between crack length to the spacing, the more the ratio is, the more the interaction is. Some cracks may be arrested.

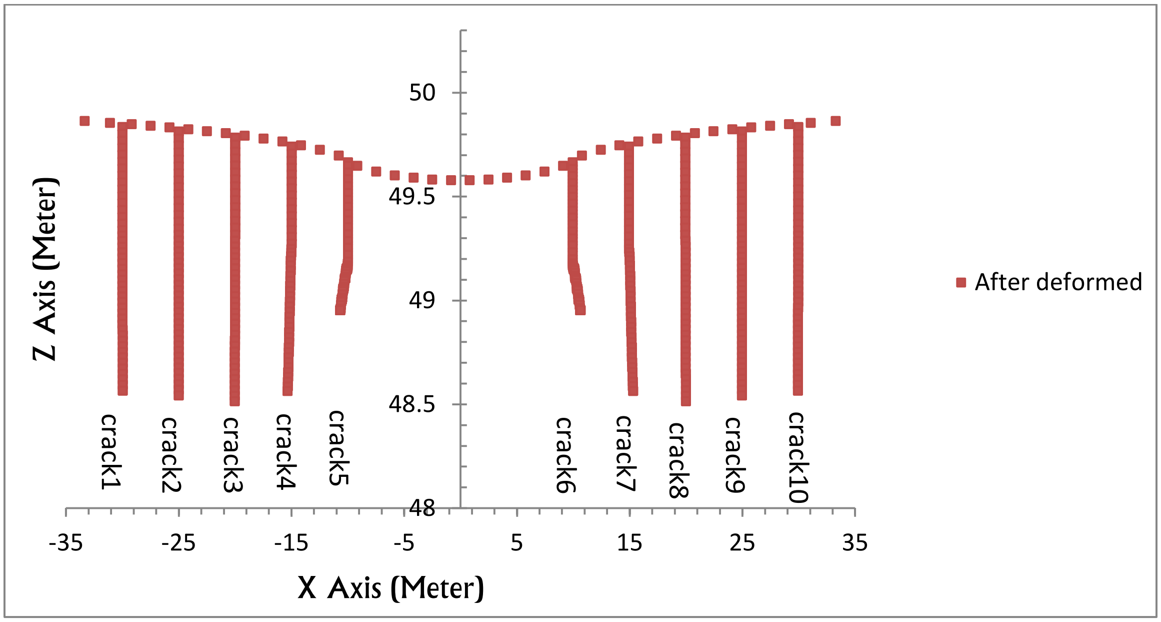

Figure 13 Two sets of crack with a spacing pressurized at the domain between -10 to 10 in 10 steps with accelerate crack growth at 0.08.

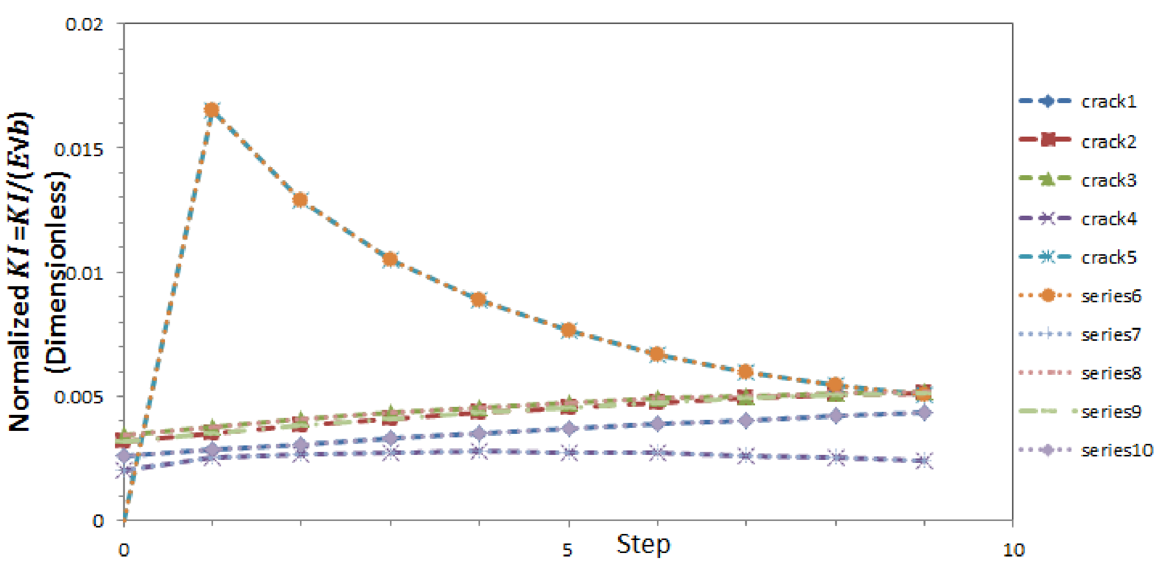

Figure 14 K1 in cracks in 10 steps with accelerate crack growth at 0.08, series 1 to 10 is from left to right cracks.

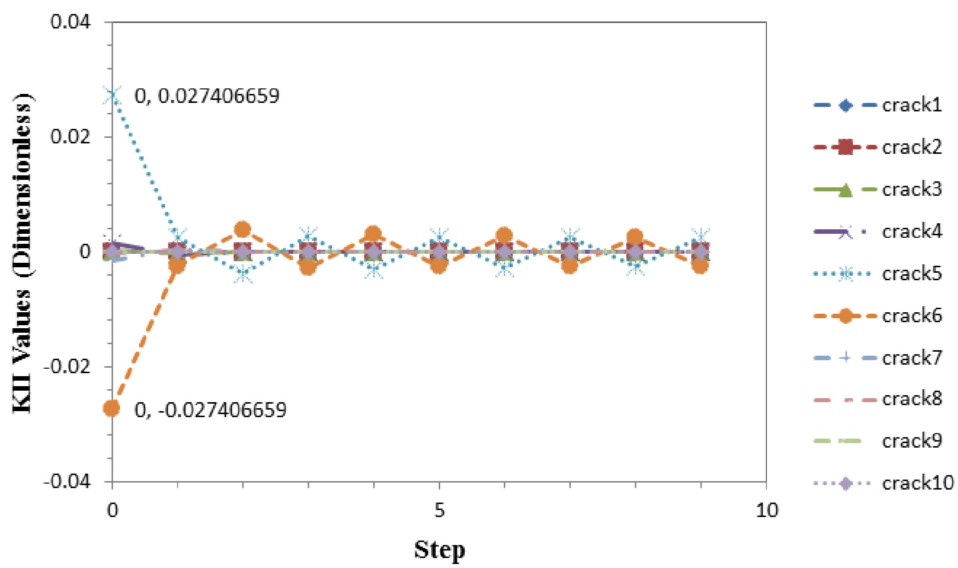

Figure 15 KII in cracks in 10 steps with accelerate crack growth at 0.05, series 1 to 10 is from left to right cracks.

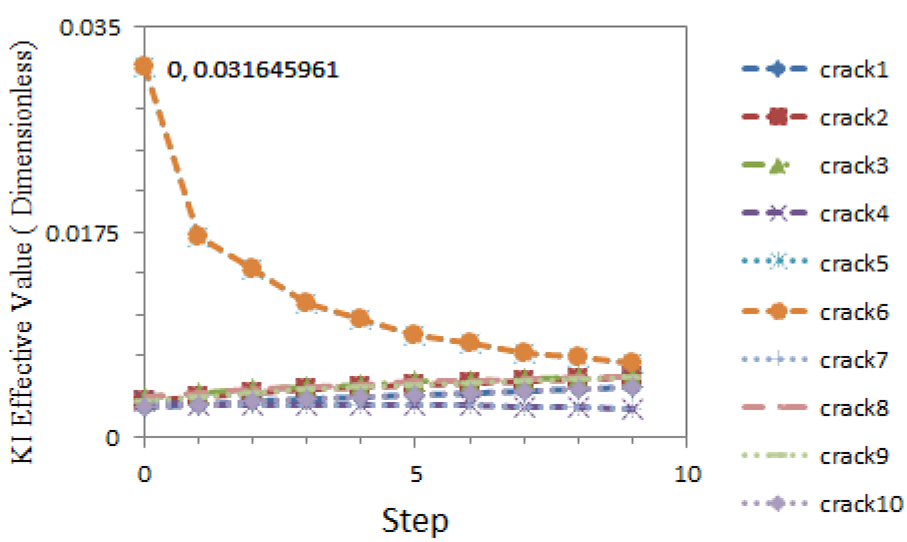

Figure 16 KI effective in cracks in 10 steps with accelerate crack growth at 0.05, series 1 to 10 is from left to right cracks.

Third, we consider a case with 10 cracks, two sets each of 5 cracks beside a pressured zone with in the middle on the top surface, and the pressurized zone has a inclined pre-existing crack in the middle, as shown in Figure 4-10. The pressured space is from -10 to 10. The outside crack would extend a larger driving force than those inside ones. The two most inner cracks at the edge of loading kink out under mixed KI and KII, and propel away from the direction of pre-existing inclined crack. Crack#4 and crack#7 were mainly arrested and closed. Crack (# 1, # 2, and # 3) and Crack (# 8, # 9, and # 10) will depend on the ratio between crack length to the spacing, the more the ratio is, the more the interaction is. Some cracks may be arrested.

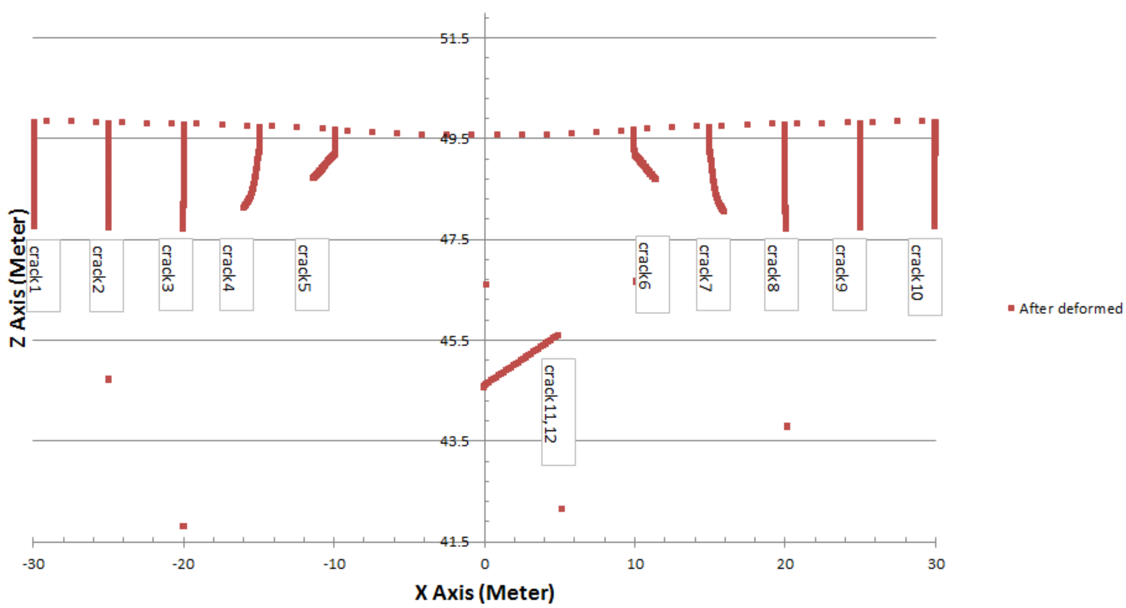

Figure 17 Two sets of crack and a main slanted pre-existing crack with a spacing pressurized at the domain between -10 to 10 in 20 steps with accelerate crack growth at 0.08.

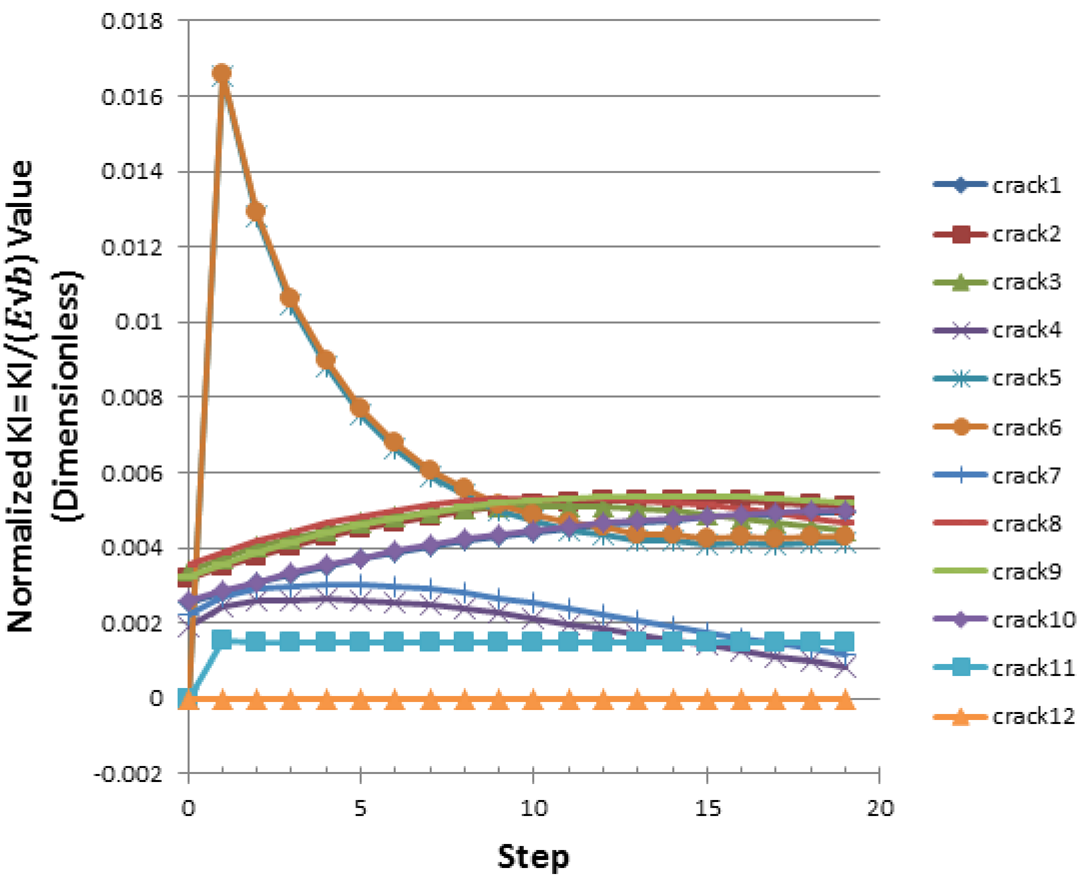

Figure 18 KI value in two sets of crack and a main slanted pre-existing crack with a spacing pressurized at the domain between -10 to 10 in 20 steps with accelerate crack growth at 0.08. Crack from 1 to 10 is the initial cracks from left to right. Crack 11 is half of the crack for the slanted crack and crack 12 is the other part of the slanted crack.

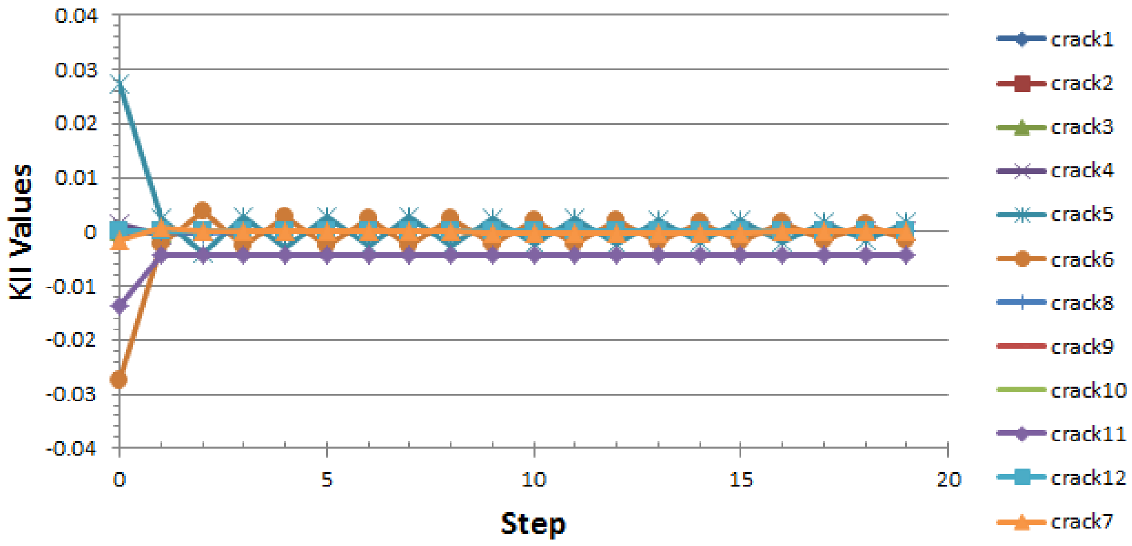

Figure 4-19 KII value.

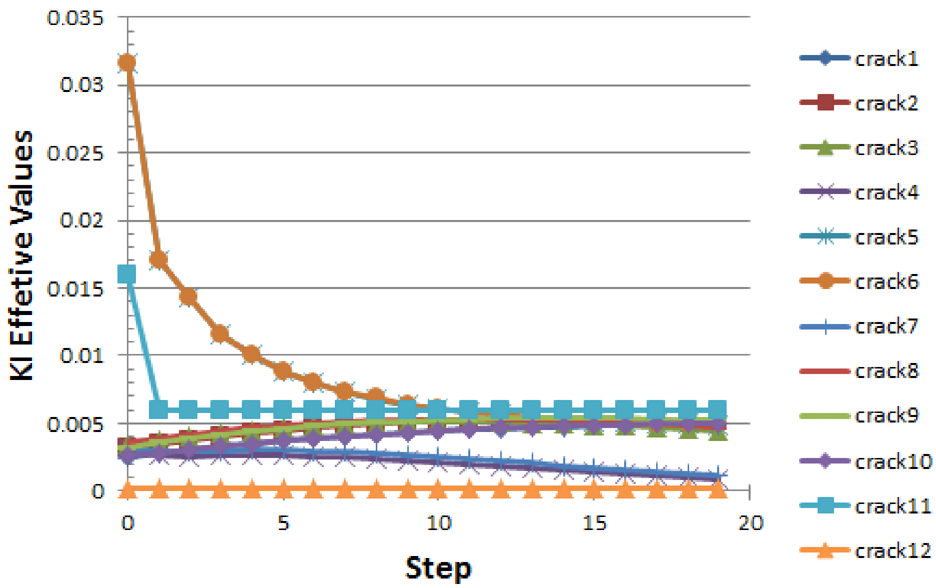

Figure 20 KI effective values in two sets of crack and a main slanted pre-existing crack with a spacing pressurized at the domain between -10 to 10 in 20 steps with accelerate crack growth at 0.08. Crack from 1 to 10 is the initial cracks from left to right.

Chapter 5

Conclusions

We have carried out modeling and simulation of multiple cracks under hydraulic loading, pertinent to the fracking process in shale rocks. The LEFM is used to approach a crack in the brittle material, and the MTS criterion is utilized to predict crack advance direction under mixed-mode loading. The single-domain dual element method is applied to solving the degeneration problem of a cracked structure. In the LEFM method, the tip-node rule is applied to evaluate the stress intensity factor accurately. Based on the analysis, we draw some conclusions as follows:

- Cracks underneath a pressurized zone, if any, are closed and do not permit fluid to flow in, and thus are mainly arrested. Such cracks can only grow slightly by the wing-crack development mechanism.
- In contrast, cracks beside a pressurized zone are opened, and experience a large driving force. It suggests that a nonuniform pressure loading is desired to drive hydraulic fracturing.
- Growing cracks interact with each other. When crack length to spacing ratio increases, the interaction gets stronger. It may result in arrest of some cracks.

- A preexisting crack may affect growing cracks significantly. Based on the simulation, growing cracks tend to avoid a transverse crack ahead on the way.

References

[1] Azadeh Riahi and Branko Damjanac. Numerical Study of Interaction Between Hydraulic Fracture and Discrete Fracture Network, Effective and Sustainable Hydraulic Fracturing, Dr. Rob Jeffrey (Ed.), ISBN: 978-953-51-1137-5, InTech, DOI: 10.5772/56416. 2013.

[2] Dershowwitz W. S. Einstein H.H., Characterizing Rock Joint Geometry with Joint System Models. Rock Mechanics and Rock Engineering, 1, 21-51. 1988.

[3] Olson J. E., Joint Pattern Development: Effects of Subcritical Crack Growth and Mechanical Crack Interaction, Journal of Geophysical Research, 98(B7), 251-265. 1993.

[4] Renshaw C.E., Pollard D.D., Numerical simulation of fracture set formation: A fracture mechanics model consistent with experimental observations, Journal of Geophysical Research- Solid Earth, 99(B5): 9359-9372. 1994.

[5] Mao Bai, Arturo Diaz, John McLennan and Juan Reyna Importance of Fracture Closure to Cuttings Injection Efficiency, Effective and Sustainable Hydraulic Fracturing, Dr. Rob Jeffrey (Ed.), ISBN: 978-953-51-1137-5, InTech, DOI: 10.5772/56070, 2013.

[6] Jaber Taheri Shakib Numerical modeling of hydraulic fracture propagation: Accounting for the effect of stresses on the interaction between hydraulic and parallel natural fractures, Egyptian Journal of Petroleum Volume 22, Issue 4, Pages 557–563, December 2013.

[7] Xi Zhang and Rob Jeffrey Development of Fracture Networks Through Hydraulic Fracture Growth in Naturally Fractured Reservoirs, Effective and Sustainable Hydraulic Fracturing, Dr. Rob Jeffrey (Ed.), ISBN: 978-953-51-1137-5, InTech, DOI: 10.5772/56405, 2013.

[8] Dimitry Chuprakov, Olga Melchaeva and Romain Prioul Hydraulic Fracture Propagation Across a Weak Discontinuity Controlled by Fluid Injection, Effective and Sustainable Hydraulic Fracturing, Dr. Rob Jeffrey (Ed.), ISBN: 978-953-51-1137-5, InTech, DOI: 10.5772/55941, 2013.

[9] Zuorong Chen An ABAQUS Implementation of the XFEM for Hydraulic Fracture Problems, Effective and Sustainable Hydraulic Fracturing, Dr. Rob Jeffrey (Ed.), ISBN: 978-953-51-1137-5, InTech, DOI: 10.5772/56287, 2013.

[10] Hyunil Jo and Robert Hurt Testing and Review of Various Displacement Discontinuity Elements for LEFM Crack Problems, Effective and Sustainable Hydraulic Fracturing, Dr. Rob Jeffrey (Ed.), ISBN: 978-953-51-1137-5, InTech, DOI: 10.5772/56445, 2013.

[11] Griffith, A. A. The phenomena of Rupture and Flow in Solids. Philosophical transactions/ Royal Society of London, ser. A, v.221, 1920.

[12] Westergaard, H. Bearing pressures and cracks, J. Appl. Mech. 61, 1939.

[13] Cheng D. Cheng D.T. Alexander H. Heritage and early history of boundary element method. Engineering analysis with boundary elements, 29:268-302, 2005.

[14] Alibadi, M. H. Boundary element formulations in fracture mechanics, Applied Mechanics Reviws 50, 83-96, 1997.

[15] Dimitry Chuprakov, Olga Melchaeva and Romain Prioul Hydraulic Fracture Propagation Across a Weak Discontinuity Controlled by Fluid Injection, Effective and Sustainable Hydraulic Fracturing, Dr. Rob Jeffrey (Ed.), ISBN: 978-953-51-1137-5, InTech, DOI: 10.5772/55941, 2013.

[16] James Kear, Justine White, Andrew P. Bunger, Rob Jeffrey and Mir- Akbar Hessami Three Dimensional Forms of Closely-Spaced Hydraulic Fractures, Effective and Sustainable Hydraulic Fracturing, Dr. Rob Jeffrey (Ed.), ISBN: 978-953-51-1137-5, InTech, DOI: 10.5772/56261, 2013.

[17] Joel Adams and Clem Rowe Differentiating Applications of Hydraulic Fracturing, Effective and Sustainable Hydraulic Fracturing, Dr. Rob Jeffrey (Ed.), ISBN: 978-953-51-1137-5, InTech, DOI: 10.5772/56114, 2013.

[18] Dimitry Chuprakov, Olga Kresse, Xiaowei Weng, Romain Prioul and Charles Cohen. Effect of Flow Rate and Viscosity on Complex Fracture Development in UFM Model, Effective and Sustainable Hydraulic Fracturing, Dr. Rob Jeffrey (Ed.), ISBN: 978-953-51-1137-5, InTech, DOI: 10.5772/56406, 2013.

[19] Xiaoxi Men, Chun'an Tang, Shanyong Wang, Yongping Li, Tao Yang and Tianhui Ma Numerical Simulation of Hydraulic Fracturing in Heterogeneous Rock: The Effect of Perforation Angles and Bedding Plane on Hydraulic

Fractures Evolutions, Effective and Sustainable Hydraulic Fracturing, Dr. Rob Jeffrey (Ed.), ISBN: 978-953-51-1137-5, InTech, DOI: 10.5772/56012, 2013.

[20] Varahanaresh Sesetty and Ahmad Ghassemi Numerical Simulation of Sequential and Simultaneous Hydraulic Fracturing, Effective and Sustainable Hydraulic Fracturing, Dr. Rob Jeffrey (Ed.), ISBN: 978-953-51-1137-5, InTech, DOI: 10.5772/56309, 2013.

[21] F. Zhang, N. Nagel, B. Lee and M. Sanchez-Nagel Fracture Network Connectivity — A Key To Hydraulic Fracturing Effectiveness and Microseismicity Generation, Effective and Sustainable Hydraulic Fracturing, Dr. Rob Jeffrey (Ed.), ISBN: 978-953-51-1137-5, InTech, DOI: 10.5772/56302, 2013.

[22] B. Yang and K. Ravi-Chandar, Efficient evaluation of elastic T-stress by the stress difference method, Engineering Fracture Mechanics 64, 589-605, 1999.

[23] B. Yang and S. Mall, On crack initiation mechanisms in fretting fatigue, ASME Journal of Applied Mechanics 68, 76-80 , 2001.

[24] Nuismer, R. J. An energy release rate criterion for mixed mode fracture, International Jounral of Fracture 11, 245-250, 2013.

[25] B. Yang and K. Ravi-Chandar, A single-domain dual-boundary-element formulation incorporating a cohesive zone model for elastostatic cracks, International Journal of Fracture 93, 115-144 ,1998.

[26] Hay Mechanical testing of Shale by instrumented indentation, Mewbourne School of Petroleum and Geological Engineering, Mewbourne College of Earth and Energy, University of Oklahoma Norman, OK, 2005.

Biographical Information

The author of this work obtained his undergraduate degree at Chun Yuan Christian University, Taiwan. His area of specialization was production Engineering with emphasis in Computer Aided Design, Industrial Engineering and Manufacturing Technology. After obtaining his bachelor degree, he served in the R.O.C Army, Taiwan, as a corporal responsible for communication with ten soldiers and one commander , and attended Han-Quan military drill(the largest military drill in Taiwan). Since August 2012. He has been working on his graduate program in Mechanical Engineering at the University of Texas at Arlington. He areas of interest include Finite Element Methods, Fracture Mechanics, and Composite Materials.